Nuclear-charge and positron-energy dependence of the single-quantum annihilation of positrons

J. C. Palathingal
Physics Department, University of Puerto Rico, Mayaguez, Puerto Rico 00680

P. Asoka-Kumar, K. G. Lynn, and X. Y. Wu
Physics Department, Brookhaven National Laboratory, Upton, New York 11973
(Received 8 September 1994; revised manuscript received 24 October 1994)

We report an experimental study of the single-quantum annihilation of positrons in a number of elements having atomic numbers between 49 and 90, utilizing a monoenergetic positron beam. Measurements were made of the differential cross sections for the forward direction for the K, L, and M atomic shells in targets of Th, Pb, Au, Hf, Gd, and In, having thicknesses that vary between 2.7 and 4.4 mg/cm^2. A shielded HPGe detector of high relative photopeak efficiency was used for recording the photon spectrum. Values for the individual atomic shells were obtained in the positron kinetic-energy range 1.02–2.24 MeV. It was observed that the differential cross sections measured for the forward direction varied with energy for each major shell almost alike so that the shell ratios appeared to remain constant while the positron energy varied. The dependence of the cross section on the atomic number Z of the target element was tested for each of the major shells at various energies of measurement. It was seen that the cross sections follow a Z^{ν} relation with $\nu \approx 5.1$ as the exponent for the K shell. For the higher shells, the exponent is approximately 6.4, which is significantly larger. It was also noted that this pattern is fairly independent of the positron energy. The results on the Z dependence are seen to be clearly at variance with the most updated theoretical predictions.

PACS number(s): 34.90.+q, 78.70.Bj

I. INTRODUCTION

The phenomenon of the single-quantum annihilation (SQA) of positrons, significant as a fundamental process of electrodynamics, was predicted by Fermi and Uhlenbeck [1] in 1933. It was explored theoretically by others in the following years [2–5], but was studied very little experimentally for a long time owing to practical limitations. As empirical observations of reasonable accuracy subsequently became feasible [6-8], matching advances were made on the theoretical front [9–13] involving significant refinements in the calculations. Despite such progress, several major predictions of theory remained empirically untested. The experimental data that were available for a long time [6–8, 14–16] had suffered from a number of disadvantages and only provided rough values of the integral cross sections. The atomic shells were not distinctly resolved. Besides, significant parameters such as the atomic shell and subshell ratios of the cross sections and the directional distributions of emission of the annihilation radiation were not subjected to experimental scrutiny.

II. THEORETICAL REVIEW

The pioneering theoretical works on the single-quantum annihilation of nonrelativistic [1] and relativistic [2–4] positrons were based on the Born approximation and the point-Coulomb potential. This approach demonstrated that the dependence of the total cross section of the SQA process on the atomic number Z of the target element could be expressed in the form

$$\sigma \sim Z^{\nu}, \tag{1}$$

with ν taking the value 5. Jaeger and Hulme [5] introduced a major improvement in the accuracy of the theoretical study and, employing a partial-wave formulation, made relativistic computations of the K-shell cross section for lead. Johnson, Buss, and Carroll [9] made more comprehensive calculations that provided the dependence of the K-shell SQA cross sections on the atomic number of the annihilating medium and the energy of the positrons. The directional distribution of the radiation was worked out for the K shell by Johnson [10], employing relativistic Coulomb wave functions. The cross-section calculations were extended by Sheth and Swamy [11] to include the LI subshell and by Broda and Johnson [13] to allow for screening effects. Screening was taken into account by using bound-state wave functions and central potentials characteristic of the relativistic Hartree-Fock-Slater atomic model. Broda and Johnson evaluated the differential cross sections for the K shell and the three L subshells and computed the polarization correlations of the annihilation radiation.

In refining and extending an earlier calculation [10] based on the simple Coulomb potential so as to include the effects of screening, Broda and Johnson [13] observed that the screening correction is generally not negligible even for the K shell, especially for low positron energy and for large atomic number of the target. In their extensive computations, the interactions of the positron and

the bound electron with the radiation field were treated in accordance with the lowest-order perturbation theory. The differential SQA cross section is expressed as

$$\frac{d\sigma}{d\Omega}=\frac{\alpha}{2\pi\hbar}\frac{E}{p}E_\gamma|T_{fi}|^2 , \tag{2}$$

where α represents the fine-structure constant and $\hbar$ Planck's constant. The incident positron has total energy E and momentum p. The energy of the SQA photon is E_γ. The matrix element T_{fi} is written in the form

$$T_{fi}=\int d^3x v^\dagger_{p\lambda}(\mathbf{x})\boldsymbol{\alpha}\cdot\mathbf{A}^*(\mathbf{x})u_B(\mathbf{x}) , \tag{3}$$

in which $v_{p\lambda}(\mathbf{x})$ and $u_B(\mathbf{x})$ represent the four-component wave functions for the positron and the bound electron, respectively, α is the Dirac spin matrix, and $\mathbf{A}(\mathbf{x})$ the spatial part of the wave function of the emitted photon. The subscript λ of the positron wave function denotes the spin projection.

With the energy of nuclear recoil neglected, the photon energy is obtained from the requirement of energy conservation as

$$E_\gamma=E+mc^2-|\epsilon| , \tag{4}$$

where ϵ represents the binding energy of the atomic electron.

The calculational procedure following Eq. (2) involves describing the positron wave function by a partial-wave expansion in angular momentum eigenstates. A summation is made over the magnetic substates of the atomic electron. For the situation in which the photon polarization is not to be observed, a summation is done also over the photon spin states. Numerical programs are hence constructed for the solution of the radial part of the positron wave function and for the partial-wave phase shifts and normalization factors in an arbitrary non-Coulomb central potential, leading to the evaluation of the differential and total cross sections.

III. EXPERIMENTAL BACKGROUND

The earliest experimental investigations of the single-quantum annihilation of positrons [6–8] resulted in the detection of the annihilation radiation and a determination of the variation of the cross section for a number of positron kinetic energies, leading up to 1500 keV, and elements of atomic number between 50 and 92. These experiments were valuable for comparing the accuracy of the existing theoretical calculations. Subsequent experiments [14–16] yielded additional data on the variation of the total cross section with positron energy and the atomic number of the target. The results were compared with the updated calculations [9].

All the experiments mentioned above were conducted by employing radioactive sources of positrons. The energy of the positrons was selected spectroscopically. The intensity could not be high. The photons were detected by NaI(Tl) scintillators coupled to photomultiplier tubes through light pipes, which are systems that could not have high energy resolution. The targets used had to be thick, 30 mg/cm^2 or over, in order to derive reasonably adequate SQA event rates. Such target thicknesses, however, could lead to line broadening in the experimental photon spectrum and also cause a large extent of positron straggling within the target, especially at the lower positron energies studied. This could make a measurement of the differential cross sections in particular not feasible because the directional distribution of the annihilation quanta is known to be extremely sharp. Further, the poor energy resolution of the detectors made it practically impossible to resolve clearly the annihilation photons of the various atomic shells. The background rates were large and the possible statistical accuracies were not high.

The first high-resolution study of the phenomenon to our knowledge was made only recently [17]. In this experiment, which was performed by the present authors and was confined to lead, monoenergetic positrons were derived from an accelerator, with energy varying between 1 and 2 MeV. A HPGe detector of 45% relative photopeak efficiency (defined conventionally for 1.33 MeV, relative to a cylindrical NaI detector of diameter 7.6 cm and length 7.6 cm for a source-detector distance of 25 cm) was engaged for observing the photons. This investigation led to a clear resolution of the shell effects and yielded the shell ratios L:K and M:K. An analysis of the L peak also gave the subshell ratio for the L shell, namely, $(L_{\rm II}+L_{\rm III})$:L. Further, the study provided the first experimental data on the directional distributions of the annihilation radiation, for the three major shells. The present measurements were done in continuation of this high-resolution experiment and have yielded data for the cross-section dependence on the positron energy and the target atomic number for the K, L, and M shells individually.

IV. DESCRIPTION OF THE EQUIPMENT

A. Positron beam

The experiment was conducted at the Brookhaven National Laboratory Dynamitron facility [18]. Positrons derived from a ^{22}Na source of strength $\sim$100 mCi are incident on a W(100) transmission moderator of thickness $\sim$6000 Å and the thermalized positrons emitted by the moderator are accelerated by a high-voltage source of the standard Cockcroft-Walton design. A collimated monoenergetic positron beam of diameter $\sim$1 mm and angular divergence less than 1° at the focal point and energy spread below 0.2% is available at the facility in the energy range 0.5–3.0 MeV. The intensity of the beam depended somewhat on the energy setting and for the present measurements, it ranged from 2.5×10^5 to 3.5×10^5 e^+/s. The beam was focused onto the target foil, which was positioned on the axis of the beam tube. The emergent beam was terminated in an adequately thick stopper of polythene (a low-Z material) that was mounted 6 mm beyond the target (Fig. 1). The inside of the beam tube was provided with a 10-mm-thick cylindrical lining of the plastic in the region of proximity to the target in order to eliminate possible SQA emissions from the steel walls of the tube on account of stray positrons.

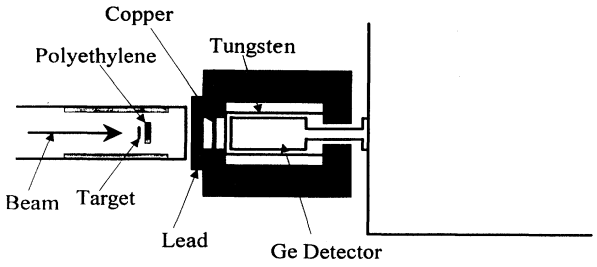

FIG. 1. Illustrative sketch of the experimental geometry (not to scale).

B. Photon detector and experimental geometry

A HPGe detector with a relative photopeak efficiency of approximately 75% (at 1.33 MeV) was engaged in recording the photon spectrum in the current series of our investigations. The measurements were all done at an angle of 0° (the forward direction). Accordingly, the detector was mounted coaxially with the beam, with its front face at a distance 16.55 cm downstream from the target (the semiangle of acceptance was 12.2°). The HPGe detector was surrounded by a 5.1-cm-thick cylindrical lead-shield assembly, lined inside with a 0.3-mm-thick roll of tungsten sheet. In order to reduce the integral count rates, a 6.35-mm-thick lead shield lined on the detector side with a copper sheet of thickness 0.635 mm was placed between the target and the photon detector. The amplifier output signal rates (above the discriminator setting) were hence limited to always be below 1500 Hz.

C. Targets

The targets of the six elements employed in the experiment were procured from Goodfellow Corporation and were of minimum chemical purity 99.9%. The thickness of each, represented in mg/cm^2 in parentheses, U(2.74), Pb(3.59), Au(3.79), Hf(4.40), Gd(3.77), and In(3.47) was small enough to ensure that the positron energy spread caused by the target was only a few keV and the mean scattering angle [19] introduced before the annihilation would not be large and could be taken into account accurately. The geometry factor giving the average divergence of the detected SQA photons relative to the directions of the annihilated positrons, represented by a term $(\cos\theta)_{av}$, had values around 0.98 for the different data and were determined with a precision of 0.003.

V. PROCEDURE

A. Measurement of the beam intensity

Since the positron rate could vary somewhat during an experimental run lasting several hours, an integral of the intensity for each run period had to be determined. The 511-keV annihilation photon peak that showed up very prominently in every spectrum could be used as a measure of the integral intensity. The peak area had to be properly calibrated however, and this was accomplished by having the beam wholly deflected onto a plastic scintillation detector, which could yield the integral positron rate. In the normal course, the beam passed through 5-mm holes in two plastic scintillators functioning as active collimators that served to monitor the beam stability, which was found quite satisfactory. The beam-intensity calibration could be checked by a calculation of the expected photopeak rate for the 511-keV photons, taking into account the absolute photopeak efficiency of the detector in the experimental geometry.

B. Photopeak calibration

The absolute photopeak efficiencies of the detector for the different photon energies involved were determined by employing radioactive sources ^{226}Ra and ^{24}Na of predetermined strengths. A graphic plot was made for the efficiency as a function of the energy of the photons emitted by the calibration sources and a polynomial fit was applied, which could be used to evaluate the efficiency corresponding to any SQA photon energy involved in the experiment (Fig. 2). Whereas the ^{226}Ra source covered photon energies in the range 600–2450 keV, the ^{24}Na source enabled the measurements to be extended to 2754 and 3867 keV. With the uncertainties in the calibration of the sources and the relative yields of the photons taken into account, a net accuracy of 2.5% is prescribed for the efficiency determinations up to 2754 keV. The probable accuracy of the efficiency curve beyond 3000 keV could be considerably less.

C. Acquisition of the spectral data

The experiment was conducted at positron energies close to 1.02, 1.30, 1.52, 1.78, 1.98, and 2.24 MeV. The exact beam energy to be set for each run was predetermined so that no natural background line could overlap significantly with any of the SQA peaks. Despite provid-

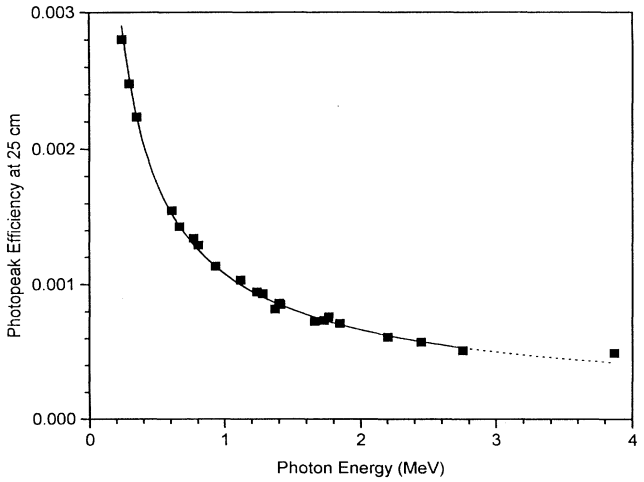

FIG. 2. Plot for the measured photopeak efficiency of the HPGe detector for a source-detector distance of 25 cm. Since the photon yield of the 3867-keV line of ^{24}Na is not known accurately, the plot and the polynomial fit are made with this energy excluded. The dotted region of the graph represents an extrapolation of the fit.

ing a 5.1-cm-thick lead shield for the HPGe detector, several natural radiation lines appeared very clearly in the spectra (Figs. 3 and 4). Long ($\sim$100-h) data runs were therefore made without the positron beam that enabled the determination of the room-background peak rates to be used in making corrections for any partial overlap with the SQA lines.

VI. SPECTRAL FEATURES

The major contributors to the recorded photon spectrum might be listed as follows: (i) the natural radioactivity, (ii) the 511-keV photons from the positron annihilation at rest, (iii) the bremsstrahlung, (iv) the two-quanta annihilation of positrons in flight (TQAF), and (v) the single-quantum annihilation. The level of γ radiation produced by the operation of the Dynamitron was negligible. The natural radioactivity was the sole contributor to the background in the SQA photon energy region, other than pulse pileup. All the other photons were of lower energy, including the photons emitted in the TQAF process. In the latter case, only one of the two photons emitted in a single event had a chance of being detected. Both could not be detected because the acceptance angle of the detector was 24.4° and the minimum angle between the directions of emission of the two TQAF photons [4] was considerably larger for any of the SQA data runs.

The energy resolution of the HPGe detector at the signal rates related to the experiment and a 3-μs integration-time setting of the signal amplifier (ORTEC 572) was found to be 1.9 keV at 1.33 MeV. The SQA peaks had widths (full width at half maximum) larger than the widths of the natural background peaks (Fig. 4) because of the spread in positron energy introduced within the target and the finite width of the incident beam energy ($\simeq$0.2%). The target thickness introduced an energy spread [19] typically about 1 keV per mg/cm^2. It is obvious that, despite the noticeable peak broadening, the finite-energy resolution of the detector was quite adequate for resolving the K, L, and M peaks of the spectra.

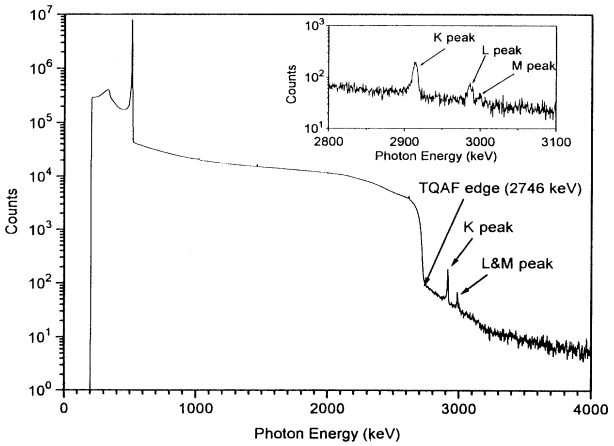

FIG. 3. Illustrative spectrum obtained with the lead target at 1989-keV positron kinetic energy. The spectrum calibration peaks corresponding to the 511-keV annihilation radiation and the 1461- and 2614-keV emissions of ^{40}K and ^{208}Bi, respectively (natural background lines), are visible in the spectrum. The 1022-keV pileup is also seen.

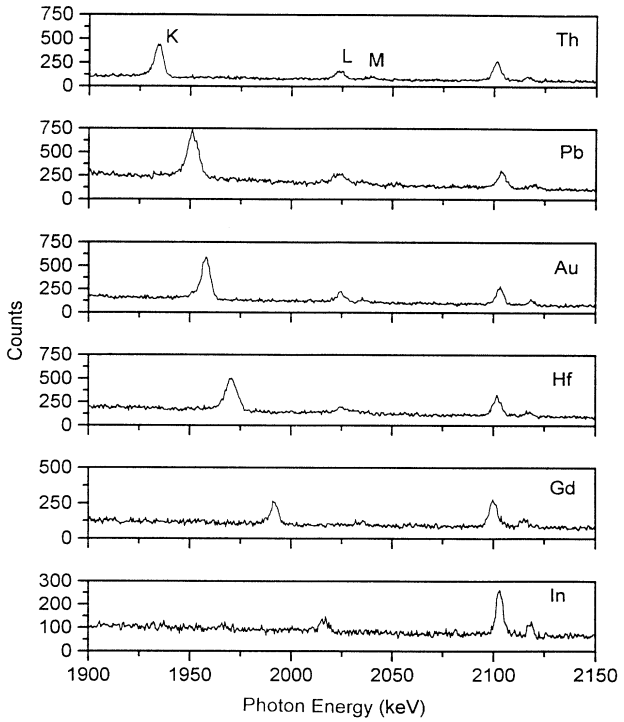

FIG. 4. Regions of the spectra for position kinetic energy 1.02 MeV, displaying the K, L, and M peaks of different elements. The fixed-energy peak seen at 2103 keV belongs to the single-escape events of the 2614-keV natural background radiation. Another natural background line, which is less prominent, is also visible in all the spectra at 2118 keV. The K-, L-, and M-peak positions shift toward higher energies for the lower-Z elements.

VII. ANALYSIS OF DATA

The width of the region chosen to represent a peak varied often, depending on the possible presence of other peaks in the vicinity. Due corrections were made to allow for the finite widths, and for any contribution from a natural line. The background was subtracted by assuming a linear background under each peak. A check on the statistical quality of the data was made at the end of the experiment by applying the χ^2 test on the values obtained for the ratio of the SQA count per incident positron at each energy setting for each target. It was concluded from the statistical test that the targets had no nonuniformity that could produce a noticeable effect on the data.

VIII. CORRECTIONS AND ERRORS

Appreciable corrections had to be made for the absorption of the photons in the media intervening between the target and the detector and for the spurious losses of positrons. Positrons could be lost at the beam-defining scintillator slits, in transmission, and by backscattering from the surface layer of the plastic scintillator. The electronic losses in counting also had to be taken into account. The

TABLE I. Experimental K-shell differential cross sections for the forward direction (detector angle 0°) (in mb/sr). The errors quoted allow for a net systematic component of 4%.

	Positron kinetic energy (MeV)					
Target	1.02	1.30	1.52	1.78	1.98	2.24
Th	1010(49)	1170(56)	1216(63)	1178(66)	1096(55)	1049(71)
Pb	636(30)	696(44)	772(39)	737(42)	714(36)	
Au	522(25)	540(32)	588(25)		588(30)	612(54)
Hf	335(16)	333(23)	344(18)	375(33)	362(19)	
Gd	173(15)	183(17)	209(14)	198(20)	181(14)	
In	49(09)	65(15)	65(08)	49(12)	62(07)	

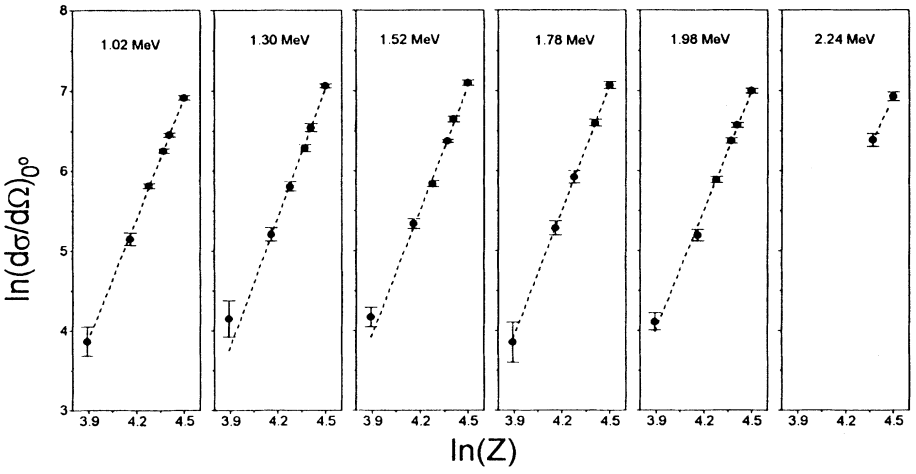

FIG. 5. Z dependence of the differential cross section for the forward direction (0° detector angle) at different positron kinetic energies for the K shell.

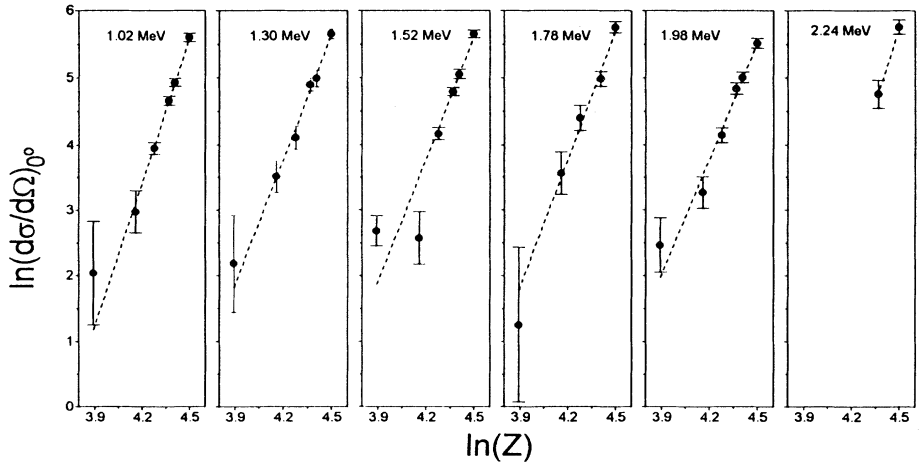

FIG. 6. Z dependence of the differential cross section for the L shell.

TABLE II. Experimental shell ratios of SQA cross sections. The L and M peaks do not show up distinctly in the In spectra because of an inadequate event rate and hence the individual L:K- and M:K-shell ratios are not presented for the element. The limits of accuracy displayed do not provide for any systematic error.

Target	L:K	M:K	$(L+M)$:K	M:L
		1.02 MeV		
Th	0.269±0.025	0.089±0.016	0.357±0.030	0.332±0.069
Pb	0.219±0.017	0.067±0.012	0.286±0.021	0.306±0.062
Au	0.204±0.019	0.070±0.013	0.274±0.023	0.342±0.076
Hf	0.156±0.018	0.067±0.013	0.223±0.022	0.428±0.110
Gd	0.119±0.046	0.000±0.032	0.120±0.056	0.004±0.240
In			0.288±0.219	
		1.30 MeV		
Th	0.245±0.024	0.073±0.018	0.318±0.030	0.297±0.086
Pb	0.213±0.036	0.108±0.028	0.321±0.046	0.505±0.166
Au	0.250±0.036	0.053±0.021	0.303±0.042	0.210±0.094
Hf	0.186±0.043	0.020±0.018	0.206±0.047	0.107±0.111
Gd	0.189±0.061	0.031±0.027	0.220±0.067	0.164±0.222
In			0.187±0.259	
		1.52 MeV		
Th	0.236±0.021	0.083±0.013	0.319±0.024	0.351±0.060
Pb	0.203±0.021	0.084±0.014	0.287±0.025	0.413±0.080
Au	0.206±0.016	0.076±0.011	0.282±0.019	0.369±0.066
Hf	0.189±0.024	0.063±0.014	0.252±0.028	0.331±0.094
Gd	0.068±0.030	0.099±0.033	0.167±0.045	1.447±0.947
In			0.314±0.147	
		1.78 MeV		
Th	0.269±0.033	0.081±0.018	0.350±0.038	0.300±0.080
Pb	0.200±0.030	0.084±0.020	0.284±0.036	0.420±0.129
Au				
Hf	0.221±0.059	0.063±0.031	0.284±0.067	0.285±0.168
Gd	0.188±0.078	0.006±0.055	0.194±0.095	0.032±0.375
In			0.098±0.248	
		1.98 MeV		
Th	0.228±0.024	0.101±0.017	0.329±0.029	0.444±0.090
Pb	0.210±0.024	0.079±0.015	0.289±0.028	0.379±0.090
Au	0.216±0.026	0.095±0.017	0.311±0.031	0.440±0.100
Hf	0.175±0.026	0.055±0.015	0.230±0.030	0.314±0.106
Gd	0.149±0.046	0.170±0.049	0.319±0.067	1.137±0.512
In			0.285±0.132	
		2.24 MeV		
Th	0.312±0.049	0.118±0.031	0.430±0.058	0.378±0.119
Au	0.199±0.057	0.082±0.040	0.281±0.070	0.413±0.253

L:K versus Z,E

Target	Positron kinetic energy (MeV) 1.02	1.30	1.52	1.78	1.98	2.24
Th	0.269(25)	0.245(24)	0.236(21)	0.269(33)	0.228(24)	0.312(49)
Pb	0.219(17)	0.213(36)	0.203(21)	0.200(30)	0.210(24)	
Au	0.204(19)	0.250(36)	0.206(16)		0.216(26)	0.199(57)
Hf	0.156(18)	0.186(43)	0.189(24)	0.221(59)	0.175(26)	
Gd	0.119(46)	0.189(61)	0.068(30)	0.188(78)	0.149(46)	

M:K versus Z,E

Th	0.089(16)	0.073(18)	0.083(13)	0.081(18)	0.101(17)	0.118(31)
Pb	0.067(12)	0.108(28)	0.084(14)	0.084(20)	0.079(15)	
Au	0.070(13)	0.053(21)	0.076(11)		0.095(17)	0.082(40)
Hf	0.067(13)	0.020(18)	0.063(14)	0.063(31)	0.055(15)	
Gd	0.000(32)	0.031(27)	0.099(33)	0.006(55)	0.170(49)	

photopeak counts were to be corrected for dead-time loss in the spectroscopy amplifier and pileup. The scattering of the positrons within the target material before the occurrence of the SQA process introduced two corrections to be considered: a small effective increase in the thickness of the target and a net increase in the directional divergence of the detected radiation over that presented by the active detector volume.

With all the significant sources of error considered, including the errors associated with the corrections, it was estimated that the positron counts were determined with a nonstatistical uncertainty of 1.9%. Taking into account the inaccuracies in the determination of photopeak efficiencies and the other smaller errors, an overall systematic uncertainty of 4% was ascribed to the absolute cross-section values. The errors in the shell ratios were accounted for almost solely by the statistical inaccuracies.

IX. RESULTS

The K-shell differential cross sections measured for the forward direction (0° detector angle) for different targets at various energies are displayed in Table I. For the L and M shells, the cross sections are given in terms of the L:K and M:K ratios (Table II). Graphic plots are made that correlate the K- and L-shell cross sections obtained at particular energies for the different targets (Figs. 5 and 6). These plots demonstrate the Z dependence of the cross sections for the different energies. Table III displays the coefficients derived from these plots for the K and L shells separately. They are compared with the theoretical predictions through a graphic illustration (Fig. 7).

X. DISCUSSION

The experiment represented accurate and extensive measurements of the single-quantum annihilation of positrons and has yielded a collection of data on the shell ratios for various targets. The differential cross section for the forward direction has been measured and the dependence of the cross section on the target atomic number and on the positron energy has been investigated in detail for the K, L, and M shells separately. The data are compared with the most comprehensive calculations that are currently available [9,10,13]. Since the forward emission accounts for much of the SQA process, a study of the differential cross section for the forward direction makes it possible to infer the general characteristics of the total cross section. It may be noted in this context that because of the acuteness of the directional distribution of the radiation at the experimental positron energies, the differential cross section observed is ~20 times larger than the average for all directions and the detector that covers only 1.16% of the total solid angle in the experimental setup receives nearly one-fourth of the emitted radiation.

In making comparisons between the experimental values of the differential cross sections and the predictions, the major handicap remaining is that the range of positron energy that has now been studied experimentally is found to be covered inadequately by theory. The largest positron kinetic energy considered theoretically has been 1.28 MeV [9]. These calculations are, however, for the total cross section only. The differential cross sections have been calculated only for kinetic energy up to 383 keV [10].

A comparison with the early experimental data is found somewhat handicapped because these data pertain only to measurements of the total cross section made with thick targets using scintillation detectors of near-2π geometry. To our knowledge, the only data available on differential cross section have been obtained by us in our exploratory work on lead [17]. The results of this earlier work are presented in Table IV along with the parallel data from the present study. It is seen that the current

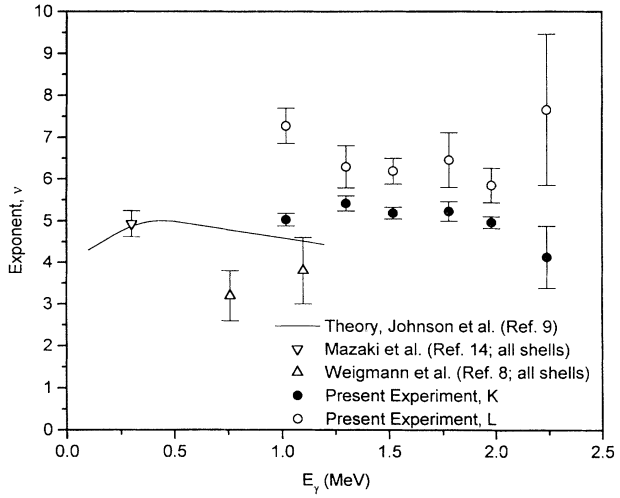

FIG. 7. Presentation of the theoretically expected values of the coefficient ν [10,14] and the experimental results. A value $\nu=5.3$ was derived for the K-shell cross sections at 300 keV by Mukoyama, Mazaki, and Shimuzu [16] from a reanalysis of the results of Mazaki, Nishi, and Shimuzu [14]. The latter group reported $\nu=4.93\pm0.31$ for the total cross section (including all shells). The two values imply that, for their work, the L-shell coefficient shall be less than 4.93 at 300 keV.

TABLE III. Experimental values of the exponent υ of Eq. (1) governing the Z dependence of the K- and L-shell cross sections at different positron kinetic energies. Indium is included in the fit for the L shell, based on the assumption that 74% of the $L+M$ yield is due to the L shell.

Energy (MeV)	υ value K shell	L shell
1.02	5.03±0.15	7.28±0.42
1.30	5.42±0.18	6.30±0.51
1.52	5.19±0.14	6.19±0.31
1.78	5.23±0.23	6.46±0.66
1.98	4.97±0.14	5.85±0.41
2.24	4.13±0.75	7.66±1.81
Average	5.13±0.07	6.39±0.19

TABLE IV. Comparison of the present experimental data on the differential cross sections and the shell ratios with the parallel results of our earlier work [17].

Reference	Energy (keV)	$(\cos\theta)_{av}$	K (mb/sr)	$L:K$	$M:K$
[17]	1007	0.960(5)	442(36)	0.23(1)	0.06(1)
This work	1020	0.974(3)	636(30)	0.22(2)	0.07(1)
[17]	1482	0.967(5)	495(54)	0.22(3)	0.07(2)
This work	1520	0.981(3)	772(39)	0.20(2)	0.08(1)
[17]	2014	0.970(5)	545(61)	0.25(3)	0.03(2)
This work	1980	0.984(3)	714(36)	0.21(2)	0.08(2)

measurement values of the differential cross sections for 0° are noticeably larger. This variation, however, can be understood in terms of the difference between the experimental geometries. As stated above, the differential cross-section plot against the angle of detection [10,17] is so steep at 0° that a variation of $\sim 2\%$ in $(\cos\theta)_{av}$ could account for the observed divergence. Calculations made on the experimental setup, with the effects of straggling of the positrons inside the target taken into consideration, have yielded the difference in the geometry factor as $1.45\pm0.58\%$ (Table IV). It may be noted in this context that in our previous measurements, although the detector was only 60% as large as the present one, the acceptance window was roughly 10% wider and the radiation was incident on the cylindrical side of the detector through a rectangular aperture. (The Pb targets employed in the two cases were of very nearly the same thickness.) It is of special interest here that, although the differential cross sections could be drastically altered by geometry variations, the shell ratios are not expected to be affected in this manner since it is known that the L- and M-shell radiations follow similarly sharp directional distributions [13,17]. The $L:K$ and $M:K$ ratios of the current measurements are hence compared with the corresponding values obtained by us earlier and excellent mutual agreement is found (Table IV).

The Z-dependence data may be viewed in the context of the predictions of theory and the experimental results published earlier. In accordance with the Born approximation, the exponent ν of Eq. (1) governing the dependence of the K-shell cross section with the atomic number Z of the target element shall have the value 5. On the other hand, the refined calculations of Johnson, Buss, and Carroll [9] predict ν to be a variant, taking the maximum value 5 at around 400 keV and decreasing nearly linearly beyond, as demonstrated graphically by Mazaki, Nishi, and Shimuzu [14] for the kinetic-energy range 200–1200 keV. Our ν values for the K differential cross section, in the range 1.02–2.24 MeV (Table III), carrying a typical statistical accuracy of a few percent, lie about a nearly constant value with an average ≈ 5.13, clearly above what may be expected from theory (Fig. 7). It is also seen from Table III that the exponent is significantly larger for the L shell. The values for the L shells indicate that they also do not vary distinguishably with energy and have an average around 6.39 for the range studied. A close look at the $L:K$ and $M:K$ ratios reveals that, whereas these tend to come down in value with the atomic number of the target, they remain relatively invariant with positron energy. This effect can be seen best from Table V, in which the average values of the ratios for all the energies studied are presented for each element and for each particular energy for all the elements. Table V also demonstrates that the $M:L$ ratio is fairly invariant with energy as well as the atomic number, remaining statistically consistent with the average value 0.34 ± 0.02. One may hence assume that the M-shell cross sections follow a Z dependence roughly the same as the L shell. Thus the ν value for the M shell could also be high.

The possibility of the forward differential cross section having a Z dependence much different from that of the total cross section can be discounted. The differential

TABLE V. Average shell ratios demonstrating the variation (a) with the atomic number of the target and (b) with the positron energy.

(a)

Z	$L:K$	$M:K$	$(L+M):K$	$M:L$
90	0.249(11)	0.087(07)	0.337(13)	0.345(32)
82	0.211(10)	0.079(07)	0.289(13)	0.369(40)
79	0.210(10)	0.075(07)	0.286(12)	0.345(40)
72	0.173(12)	0.056(07)	0.233(14)	0.298(50)
64	0.114(20)	0.051(16)	0.192(27)	0.193(142)
49			0.265(80)	

(b)

Energy (MeV)	$L:K$	$M:K$	$(L+M):K$	$M:L$
1.02	0.201(09)	0.072(07)	0.269(11)	0.328(37)
1.30	0.228(16)	0.053(09)	0.289(19)	0.244(51)
1.52	0.195(09)	0.077(06)	0.279(11)	0.367(36)
1.78	0.227(20)	0.076(12)	0.302(23)	0.318(62)
1.98	0.204(12)	0.083(08)	0.291(14)	0.405(48)
2.24	0.264(37)	0.104(25)	0.369(45)	0.384(108)

TABLE VI. Theoretical results of Johnson [10] illustrating that the differential cross section for the forward direction follows essentially the same Z dependence as the total cross section.

Energy	v	v (differential)		
(keV)	(integral)	0°	20°	29°
128	4.4	3.6	3.7	3.8
256	4.7	4.6	4.7	4.7
383	5.0	4.9	5.0	4.9

cross-section calculations of Johnson [10] reveal this aspect quite clearly. Calculations show that, at the energies involved, the differential cross section in the forward directions has essentially the same dependence on Z as the total cross section (Table VI). Thus our results on the Z dependence of the 0° differential cross section are considered to be applicable to the total cross sections as well and hence stand out as a clear deviation from the theoretical expectations. Aside form the unexpectedly high values of v observed for the K shell, the stronger dependence of the L and M cross sections on Z needs to be accounted for theoretically. It may be remembered here that the L- and M-shell contributions make up to about one-fourth of the total SQA radiation. The dependence of the shell ratios on positron energy is also a significant feature to be understood in physical terms. Although the underlying aspects have not been explored adequately by theory, these observed effects may presumably be accounted for solely in terms of the electron densities.

In common with our earlier observation [17], the measured differential cross section for the forward direction is seen to increase with positron energy for a limited region of the range of energy studied, despite the expected fall in the integral cross section. This may be understood as the result of two effects. The reduced straggling of the positrons in the target and the consequent increase in $(\cos\theta)_{av}$ for higher positron energies (Table IV) mean that the radiation yield observed along the forward directions will be larger than what may be available for a lower positron energy. An increased forward momentum of the positron also contributes significantly to an enhanced forward peaking of the emitted radiation, as demonstrated theoretically by Johnson.[10]

In view of the significance of the SQA phenomenon in heavy-ion colliders, wherein an inverse process leads to electron-positron pair formation, a close understanding of the phenomenon investigated between theory and experiment appears to be timely and significant.

ACKNOWLEDGMENTS

The present work was supported in part by the National Science Foundation through Grant No. PHY-9203873 and by the Department of Energy through Contract No. DE-AC02-76CH00016. The authors acknowledge the technical support rendered by Harry Hacker during different stages of the work.

[1] E. Fermi and G. E. Uhlenbeck, Phys. Rev. **44**, 510 (1933).
[2] H. J. Bhabha and H. R. Hulme, Proc. R. Soc. London Ser. A **146**, 723 (1934).
[3] Y. Nishina, S. Tomonaga, and H. Tamaki, Inst. Phys. Chem. Res. (Tokyo) **27**, 178 (1935).
[4] H. A. Bethe, Proc. R. Soc. London Ser. A **150**, 129 (1935).
[5] J. C. Jaeger and H. R. Hulme, Proc. Cambridge Philos. Mag. **32**, 158 (1936).
[6] L. Sodickson, W. Bowman, J. Stephenson, and R. Weinstein, Phys. Rev. **124**, 1851 (1961).
[7] H. Langhoff, H. Weigmann, and A. Flammersfeld, Nucl. Phys. **41**, 575 (1963).
[8] H. Weigmann, H. Hansen, and A. Flammersfeld, Nucl. Phys. **45**, 555 (1963).
[9] W. R. Johnson, D. J. Buss, and C. O. Carroll, Phys. Rev. **135**, A1232 (1964).
[10] W. R. Johnson, Phys. Rev. **159**, 61 (1967).
[11] C. V. Sheth and N. V. V. J. Swamy, Phys. Rev. **167**, 319 (1968).
[12] R. H. Pratt and H. K. Tseng, Phys. Rev. A **5**, 1063 (1972).
[13] K. W. Broda and W. R. Johnson, Phys. Rev. A **6**, 1693 (1972).
[14] H. Mazaki, M. Nishi, and S. Shimuzu, Phys. Rev. **171**, 408 (1968).
[15] H. Friedrich, Z. Phys. **246**, 407 (1971).
[16] T. Mukoyama, H. Mazaki, and S. Shimuzu, Phys. Rev. A **20**, 82 (1979).
[17] J. C. Palathingal, P. Asoka-Kumar, K. G. Lynn, Y. Posada, and X. Y. Wu, Phys. Rev. Lett. **67**, 3491 (1991).
[18] P. Asoka-Kumar, J. S. Greenberg, S. D. Henderson, H. Huomo, M. S. Lubell, K. G. Lynn, R. Mayer, S. McCorkle, J. McDonough, J. C. Palathingal, B. F. Philips, A. Vehanen, M. Weber, and X. Y. Wu, Nucl. Instrum. Methods Phys. Res. Sect. A **337**, 3 (1993).
[19] G. Knop and W. Paul, in *Alpha-, Beta- and Gamma-Ray Spectroscopy* (North-Holland, Amsterdam, 1968), Chap. I.